Neuron, Vol. 14, 561–569, March, 1995, Copyright © 1995 by Cell Press

Mammalian Rod Terminal: Architecture of a Binary Synapse

R. Rao-Mirotznik,*† A. B. Harkins,*‡ G. Buchsbaum,† and P. Sterling*
*Department of Neuroscience
†Department of Bioengineering
University of Pennsylvania
Philadelphia, Pennsylvania 19104

Summary

The mammalian rod synapse transmits a binary signal (one photon or none) using tonic, rapid exocytosis. We constructed a quantitative, physical model of the synapse. Presynaptically, a single, linear active zone provides docking sites for ~130 vesicles, and a "ribbon" anchored to the active zone provides a depot for ~640 vesicles. Postsynaptically, 4 processes invaginate the terminal: 2 (known to have low affinity glutamate receptors) lie near the active zone (16 nm), and 2 (known to have high affinity glutamate receptors) lie at a distance (130–640 nm). The presynaptic structure seems designed to minimize fluctuations in tonic rate owing to empty docking sites, whereas the postsynaptic geometry may permit 1 vesicle to evoke an all-or-none response at all 4 postsynaptic processes.

Introduction

Gray and Pease (1971) pointed out similarities between the photoreceptor synapse and a conventional bouton (Figure 1). They proposed, in a tour de force of structural reasoning, that the photoreceptor synaptic ribbon guides vesicles to docking sites at the presynaptic membrane, and they identified the "active zone" (the region of vesicle exocytosis) as the region where vesicles at the ribbon's basal edge touch the plasma membrane (sl). This identification was subsequently supported by the findings that exocytotic pits are restricted to this region and that the strip of presynaptic membrane directly beneath the ribbon is packed with intramembrane particles (Raviola, 1976). Similar particle concentrations at other active zones include calcium channels (e.g., Pumplin et al., 1981; Roberts et al., 1990).

On the other hand, many differences between the photoreceptor synapse and the conventional bouton are still unexplained. Why should the photoreceptor employ a ribbon plus a complex, three-dimensional synaptic cleft, while the conventional bouton lacks the fancy docking mechanism and is strictly two-dimensional? Addressing this question requires stepping beyond the "generic" photoreceptor synapse (Figure 1B) to quantitate a particular photoreceptor synapse. For this we chose the mammalian rod synapse.

In starlight (the luminance range served by the rod synapse; Smith et al., 1986), the spatiotemporal density of photons striking the retina is so low that the thin mammalian rod signals either one photon or none (Sterling et al., 1987). Although amphibian rods are coupled by gap junctions, mammalian rods are not (reviewed by Attwell, 1986; Sterling, 1990). They are coupled to cones (Kolb, 1977; Smith et al., 1986), but calculations suggest that, when there is less than one photon per rod per integration time, the rod–cone junctions uncouple to isolate the rod (Smith et al., 1986). Thus, the signal reaching the mammalian rod synapse is binary: zero or one photon.

This binary signal is encoded via an unusual mechanism. Zero is represented by tonic exocytosis, and one is represented by a pause in secretion (Dowling, 1991). Based on a model of the overall circuit, we calculated the tonic rate of transmitter release needed to convey the binary signal to be at least 40 vesicles per second, a rate much higher than that at conventional (nonribbon) synapses (Rao et al., 1994). Here we describe quantitatively several structural features of the rod terminal in cat that seem suited to this task.

Results

Rod Synaptic Architecture Is Largely Unaffected by Background Luminance

We compared quantitatively rod terminals from a light-adapted retina to those from a retina that had been dark-adapted for 2 hr. Following such prolonged dark adaptation, cat ganglion cells reach peak sensitivity and respond to single photons (Barlow et al., 1971; Mastronarde, 1983). Therefore, the rod terminal's structure after several hours of total darkness should reflect its capacity to convey a binary signal.

No differences were observed in the volume, surface area, or shape of most presynaptic and postsynaptic structures (Table 1). Nor was there any difference in the structure of the synaptic cleft (Table 1). One exception was that the presynaptic ribbon appeared slightly shorter in the dark-adapted tissue (see active zone length). Another minor exception was that the "diverticula" (infoldings of rod presynaptic membrane) were larger in this tissue; however, we found no differences comparable to those reported by others in rodent (Spadaro et al., 1978; Brandon and Lam, 1983; Vollrath et al., 1989). Those studies relied on single sections and were not quantitative. In view of the difficulties in interpreting the rod terminal's complex structure from single sections, we doubt that these earlier observations are reliable. However, in fish and turtle, changes in terminal structure with adaptation level are marked and have been established quantitatively (fish, reviewed by Wagner and Djamgoz, 1993; turtle, Schaeffer and Raviola, 1978; Abe and Yamamoto, 1988). Since, in our tissue, the differences in structure with adaptation were minor, we combined the results from both adaptive states.

‡Present address: Department of Pharmacological and Physiological Sciences, University of Chicago, Chicago, Illinois 60637.

Table 1. Measurements of the Dark- and Light-Adapted Rod Terminals

	Dark-Adapted	Light-Adapted
Presynaptic features		
Active zone length* (μm)	2.14 ± 0.19 (10)	2.52 ± 0.27 (10)
Ribbon surface area (μm²)	0.74 ± 0.13 (10)	0.80 ± 0.17 (10)
Rod "fingers" surface area (μm²)	0.26 ± 0.13 (5)	0.18 ± 0.07 (5)
Diverticula		
Surface area of each (μm²)	0.55 ± 0.40 (13)	0.27 ± 0.18 (11)
Surface area per rod* (μm²)	1.42 ± 0.61 (5)	0.60 ± 0.56 (5)
% rods with two ribbons	5.3 (75)	4.7 (260)
Postsynaptic features		
Horiz. cell process		
Volume (μm³)	0.49 ± 0.07 (10)	0.37 ± 0.08 (10)
Surface area (μm²)	5.86 ± 0.69 (10)	4.40 ± 1.06 (10)
Bip. cell dendrite		
Volume (μm³)	0.08 ± 0.02 (10)	0.08 ± 0.02 (10)
Surface area (μm²)	0.99 ± 0.26 (10)	1.10 ± 0.20 (10)
Cleft features		
Invagination depth (μm)	1.16 ± 0.12 (4)	0.91 ± 0.06 (5)
Extracellular volume (μm³)	0.21 ± 0.02 (5)	0.21 ± 0.04 (5)
Distance from active zone to bipolar dendritic tip		
Minimum (μm)	0.21 ± 0.14 (8)	0.28 ± 0.11 (10)
Maximum (μm)	1.02 ± 0.19 (8)	1.01 ± 0.24 (10)
Distance from active zone to bipolar cell surface		
Minimum (μm)	0.11 ± 0.07 (8)	0.14 ± 0.09 (10)
Maximum (μm)	0.61 ± 0.17 (8)	0.67 ± 0.19 (10)

Values are mean ± SD; numbers in parentheses are n.
*Dark- and light-adapted values were compared using the student's two-tailed t test. For active zone length, the difference was slightly, but significantly ($p < .005$), different. For diverticular surface area per rod, the difference was almost significant ($p < .1$).

Rod Terminal Contains One Presynaptic Active Zone and One Postsynaptic Tetrad

The cat rod terminal is generally supposed to contain "one or two" synaptic ribbons, each associated with a "triad" of postsynaptic processes (Boycott and Kolb, 1973; and see Figure 1B). The impression of two ribbons and two triads derives from electron micrographs of single sections that often show two separate segments of ribbon, each apparently associated with 1 bipolar cell and 2 horizontal cell processes (Figure 2A). Yet, these are misapprehensions. In serial sections, the two segments of ribbon were usually connected: 95% of the rod terminals in one cat (n = 335) contained only one ribbon (Figure 2B; Figure 3A). This was also true for 50 terminals examined in two other cats. Since the ribbon's basal edge is fitted to the active zone, there is also only one active zone. Furthermore, associated with the active zone there were invariably not 3 but 4 postsynaptic processes: 2 bipolar cell dendrites and 2 horizontal cell terminals. We term these, by extension of the standard terminology, a "tetrad."

Active Zone Is Arched and Has Many Docking Sites

As indicated in the Gray-Pease model (Figure 1B), the active zone flanks an electron-dense structure that appears to anchor the ribbon at a fixed distance (~62 nm) from the presynaptic membrane. This structure is narrow in cross-section (0.25 μm; see Figure 6 in Raviola, 1976) but long (2.3 ± 0.3 μm; n = 20) and arched (Figure 3A). Along either side of the arch, vesicles dock in two rows (see Figure 6 in Raviola, 1976). If vesicles packed tightly,

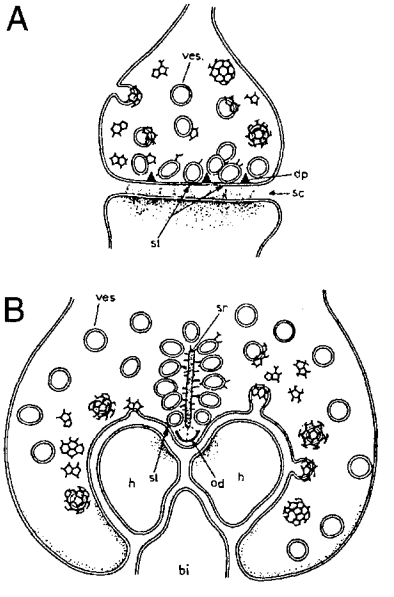

Figure 1. Generic Synapses

(A) Conventional bouton; (B) photoreceptor synapse. Generic photoreceptor synapse suggests a "triad" of postsynaptic processes and greatly underestimates the distance from vesicle docking site to bipolar cell dendrite (reprinted from Gray and Pease, 1971, with permission). ad, arciform density; bi, bipolar cell; dp, dense projections; h, horizontal cell; sc, synaptic cleft; sl, specific localities; sr, synaptic ribbon; ves, vesicle.

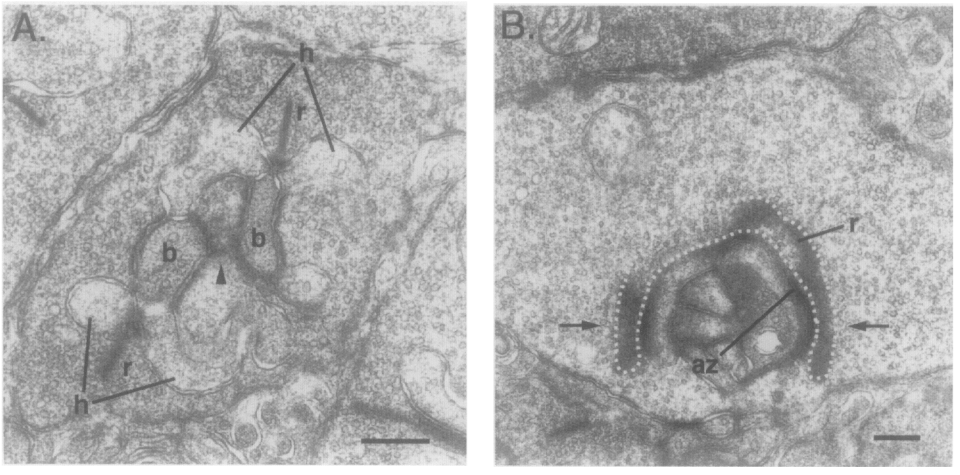

Figure 2. Single Ultrathin Sections Are Misleading

Rod terminal commonly shows two ribbon (r) profiles, each apparently associated with 1 bipolar (b) and 2 horizontal (h) cell processes (A). Such images seem to imply that the rod terminal serves two triads. However, an oblique section (B) suggests a single, crescent-shaped ribbon (dotted outline) and an arched active zone (az). (Arrows indicate plane of section that would give images resembling [A]). This was confirmed by reconstructions from successive sections (Figure 3A). Note that rod membrane apposed to bipolar cell processes stain densely. Staining is also seen at rod–rod appositions (arrowhead). Unlike in human rod (Linberg and Fisher, 1988), there was no evidence in our tissue of horizontal cell synapses onto the rod terminal. Bar, 0.3 μm.

their center-to-center spacing would be about 37 nm, and an active zone could dock up to ~250 vesicles. However, freeze-fracture images suggest that the spacing is actually 70 nm (Raviola, 1976), so the active zone probably docks ~130 vesicles. For comparison, the maximum at a conventional active zone estimated from published freeze-fracture micrographs is ~50 vesicles (Akert, 1973). Thus, docking sites at the rod active zone are at least twice as numerous as at the largest known conventional active zones. Moreover, in a rod terminal, docking sites are arranged in one dimension, whereas in a conventional bouton they cluster in two dimensions.

Presynaptic Ribbon Has a Large and Constant Surface Area

The ribbon's basal edge conforms to the arch of the active zone and tends to be crescent shaped. Although the exact shape of the ribbon varies (Figure 3A), the surface area is remarkably constant (0.77 ± 0.15 μm^2 per face; n = 20). The ribbon has long been thought to serve as a depot from which synaptic vesicles reload empty docking sites. In the present material, vesicles were tethered to both faces of the ribbon by filaments 20–30 nm long. Spacing of the tethered vesicles (center-to-center) was about 48 nm, so the ribbon's two faces accommodate ~770 vesicles. This number includes vesicles tethered to the ribbon's basal edge that are presumably docked at the presynaptic membrane. Therefore, the number of depot vesicles available to reload docking sites is ~640, and the ratio of depot sites to docking sites is about 5.

Rarely (5% of rods), a terminal had two ribbons, each with an associated active zone (Figure 3B). In such cases, total depot sites per terminal were ~660 (ribbon surface area = 0.66 ± 0.15 μm^2 per face), and total docking sites (with 70 nm spacing) were ~125 (active zone length =

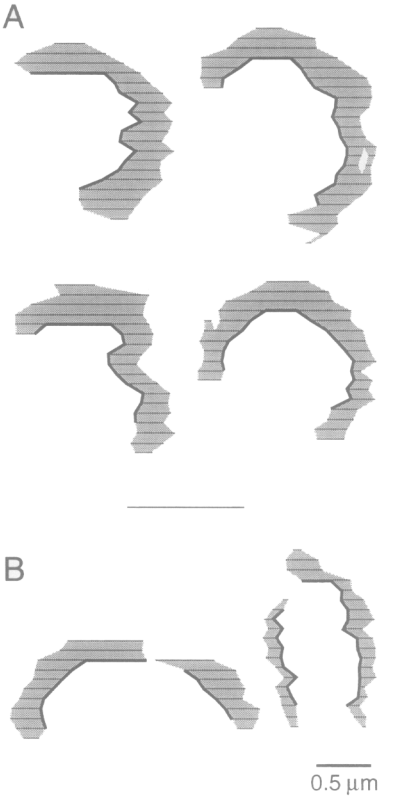

Figure 3. Synaptic Ribbons Are Crescent Shaped and of Uniform Area

(A) Reconstructed ribbons from 4 terminals. Most terminals contained only one ribbon (shaded). Invariably, it was arched and anchored to the active zone's convexity (thick line).

(B) A few terminals contained two ribbons. The total ribbon areas and active zone lengths were the same as those for single-ribbon terminals. In (A) and (B), left column shows ribbons from dark-adapted retina; right shows ribbons from light-adapted retina.

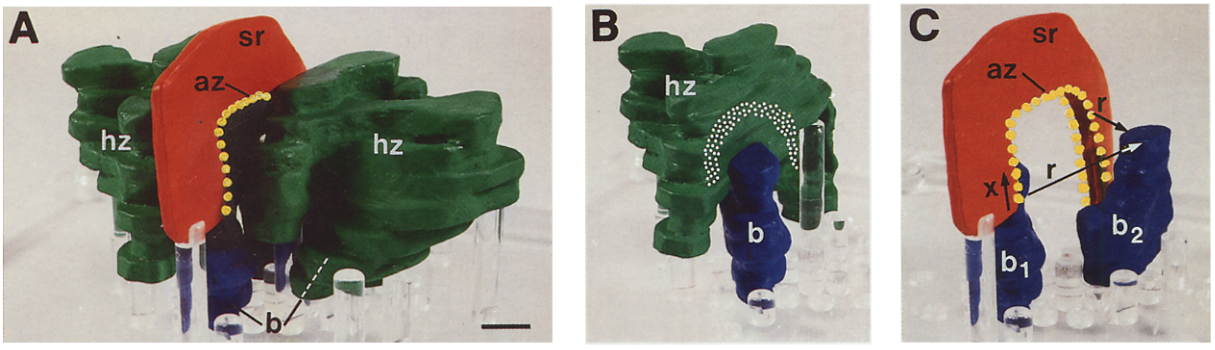

Figure 4. Three-Dimensional Model (Clay) to Scale of Rod Synapse

(A) Active zone (az) plus synaptic ribbon (sr) arch between 2 horizontal cell (hz) terminals and above 2 bipolar cell (b) dendrites (1 bipolar cell dendrite is hidden).

(B) Transmitter receptors (speckling) on the horizontal cell arch parallel to the active zone. Therefore, every vesicle docking site is near some patch of these receptors.

(C) Bipolar cell dendrites (b_1 and b_2) lie far from the active zone. x, position of docking sites along the active zone; r, distance from a given site to the bipolar cell dendrite (Figure 6 plots x versus r). Bar, 0.3 μm.

2.2 ± 0.5 μm; n = 6). These values differ only slightly from those of single-ribbon terminals. Thus, a double-ribbon terminal resembles a single-ribbon terminal in which the synaptic apparatus has been fractured. The constancy of depot and docking sites in such cases suggests that these numbers are fundamental to the specific function of the rod synapse.

Conceivably, the crescent shape of the ribbon might result from its large size. If the ribbon's material were insufficiently stiff, like sheet metal, it might simply buckle upon reaching a certain extent. However, the cat cone contains several ribbons that are considerably longer than those of the rod. These ribbons, which serve up to five separate triads, are quite straight along their basal edges with no hint of an arch (Harkins and Sterling, unpublished data). Thus, the crescent shape of the rod ribbon is probably a deliberate feature of the design.

Relationship of Active Zone to Tetrad

We considered how an elongated active zone, where transmitter is released focally, would relate to the 4 postsynaptic processes where transmitter is bound. The configuration proved hard to grasp from single sections, even though we could follow all the pieces from section to section. Consequently, we constructed a physical model (Figure 4).

Horizontal Cell Processes Are Near the Active Zone

At the mouth of the invagination (see Figure 7B), the horizontal cell process is narrow (~0.1 μm diameter), but inside the invagination it balloons and crinkles, thereby achieving considerable surface area (5.1 ± 1.2 μm^2; n = 20; Figures 4A and 4B). The process expands orthogonally to the active zone and also parallel to it (Figure 4A). The central face of the process flattens in the plane established by the ribbon (Figure 4B) to meet the flattened head of the other horizontal cell process. Just lateral to this flattened region, the process follows the arch of the active zone in close proximity (~16 nm across the cleft). Both the flattened and adjacent lateral regions of the horizontal cell process exhibit a postsynaptic density about 70–100 nm wide that parallels the active zone. This density (Figure 4B) corresponds to the strip of horizontal cell membrane with intramembrane particles (Raviola and Gilula, 1975) and presumably bears the postsynaptic receptors (e.g., Pumplin and Reese, 1978). These are glutamate receptors of the AMPA/kainate type (Massey, 1990). Thus, every synaptic vesicle docked along the extended active zone is about 16 nm from the nearest patch of AMPA/kainate receptors on the horizontal cell (summarized in Figure 5).

Bipolar Cell Dendrites Are Far from the Active Zone

The dendrites of the rod bipolar cell are oval in cross-section and untapered within the invagination (Figure 4C). This gives them a rather stout appearance and a modest surface area (1.0 ± 0.2 μm^2; n = 20). The bipolar cell's dendritic tips occupy concavities on the inferior surfaces of the horizontal cell expansions (Figure 4B).

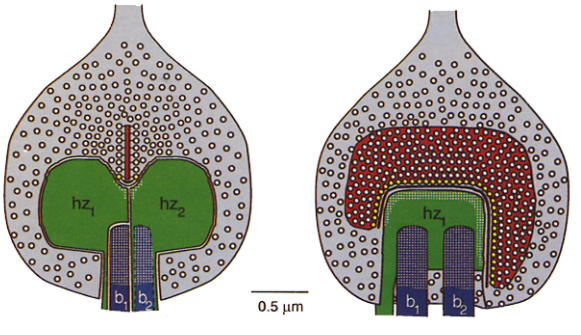

Figure 5. Summary Diagram of Rod Photoreceptor Synapse

Views of rod terminal perpendicular (left) and parallel (right) to face of ribbon. Presynaptically, a long active zone docks ~130 vesicles (yellow) and the extensive ribbon tethers ~770 vesicles. Postsynaptically, 4 processes (2 horizontal cell [hz] + 2 bipolar cell [b]) occupy the invagination; the horizontal cell receptors (white speckling) arch parallel to the active zone and thus always lie near (16 nm) the docking sites; the bipolar cell receptors (white speckling distributed over entire surface) lie far (130–640 nm) from the docking sites. (Note: the mouth of the invagination is exaggerated since, for clarity, we cut away parts of the rod.)

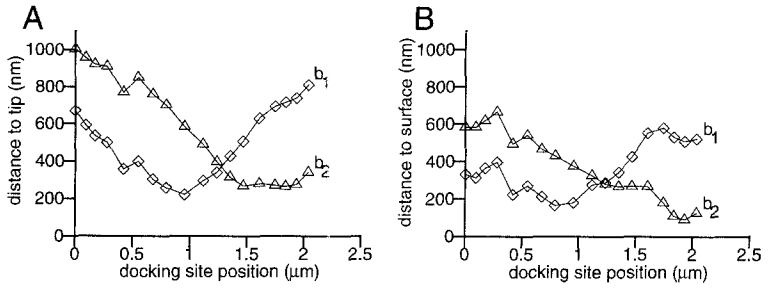

Figure 6. Distance from Active Zone to Bipolar Cell Dendrites Is Large and Variable

Position of docking site along active zone (x) versus distance (r) from that site to bipolar dendritic tip (A) and to bipolar cell surface (B) for 1 rod terminal (see Figure 4C). b_1 and b_2 indicate the 2 bipolar cell dendrites of the tetrad. The distances are much shorter and more uniform when measured to the bipolar cell surface.

Although the generic model of the photoreceptor gives the impression that a bipolar cell's dendritic tip lies directly beneath the active zone at a fixed distance (Figure 1B), this is erroneous. The dendritic tips do not nestle neatly under the arch of the active zone, equidistant from all points along it; rather, they splay out on either side, and the distance from a given point on the arch to a dendritic tip varies greatly (Figure 4C; Figure 5). For the 2 bipolar cell dendrites of 1 rod terminal, the distance ranged from 220 to 1000 nm (Figure 6A). Measured for 18 bipolar cell dendrites (9 tetrads), the distance from active zone to a tip was as near as 250 ± 130 nm and as far as 1010 ± 210 nm. If we ignored the tip and simply measured from active zone to the nearest patch of bipolar cell membrane, the distance fell markedly. For the bipolar cell dendrites of Figure 6A, this distance ranged from 90 to 660 nm (Figure 6B). Across the 18 bipolar cell dendrites, the minimum distance was 130 ± 80 nm and the maximum was 640 ± 180 nm.

The rod bipolar cell dendrites do not show any concentration of intramembrane particles (Raviola and Gilula, 1975). Thus, the distribution of postsynaptic receptors cannot be recognized by electron microscopy. However, it is known that the rod bipolar cell, depolarizing to light (Dacheux and Raviola, 1986), employs a metabotropic "APB" glutamate receptor (Yamashita and Wässle, 1991). This receptor was recently identified as mGluR6 and localized by confocal microscopy to the invaginated dendritic tip (Nomura et al., 1994; see Figure 5).

The few rod terminals with two active zones housed only one invagination associated with one tetrad of postsynaptic processes. One bipolar cell dendrite per active zone occupied each central site, and two horizontal cell processes occupied the lateral sites. Some human rods also have two ribbons, and there single invaginations are also found (Linberg and Fisher, 1988). This arrangement differs from the cone terminal, in which each of many active zones is served by a separate invagination. For rod terminals with two active zones, the extracellular volume within the invagination was essentially the same as for the single-ribbon rod terminals, and so were the distances from active zone to bipolar and horizontal cell processes.

Two Types of Rod Process Invaginate the Terminal

In every rod terminal, multiple "fingers" of rod cytoplasm protrude into the main invagination to fill the space between the 2 bipolar cell dendrites (Figure 7A). These fingers contribute about 0.2 μm^2 to the membrane surface area contained within the invagination (n = 10 terminals). In some instances, the appositions between these rod–rod fingers showed submembranous density (Figure 2A). Similar fingers were also noted in human rods (Missotten, 1965; Linberg and Fisher, 1988).

A different set of processes arises where fingers of rod

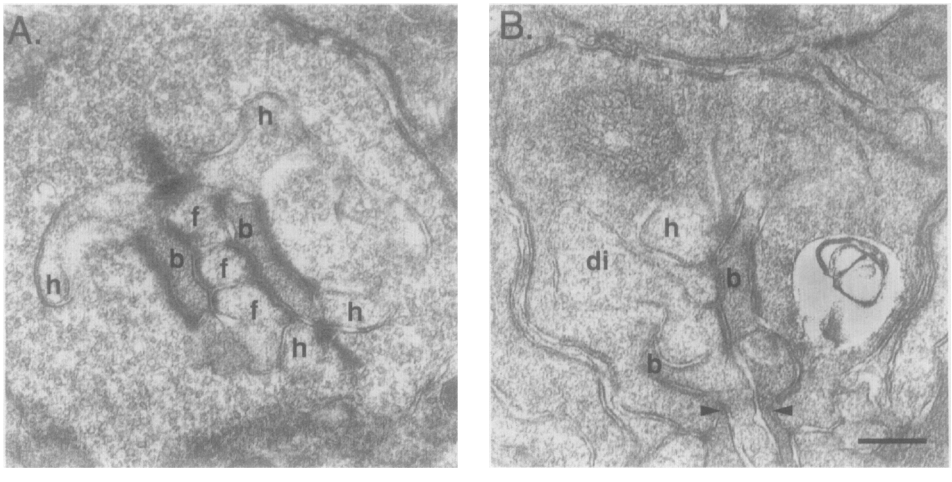

Figure 7. Electron Micrographs Showing Rod Processes That Invaginate the Rod Terminal

(A) Fingers (f) of rod cytoplasm insert between the bipolar cell dendrites (b).

(B) Diverticulum (di) shown connects to the invagination. Arrowheads indicate mouth of invagination.

cytoplasm extend from the main invagination back into the rod terminal itself (Figure 7B). Such diverticula are also present in other mammals (Cohen, 1964; Missotten, 1965; Evans, 1966). In some cases, a diverticulum could be traced to the edge of the invagination (Figure 7B); in other cases, it did not quite connect, suggesting that the diverticulum might have pinched off from the rod membrane. Every rod terminal contained 1–4 such diverticula. Their total surface area per terminal was 0.6 ± 0.6 μm^2 in the light-adapted state and 1.4 ± 0.6 μm^2 in the dark-adapted state (Table 1). Analogous structures have been seen at other photoreceptor terminals (Ripps and Chappell, 1991) and at neuromuscular junctions following treatment to induce unusually high rates of transmitter release (Ceccarelli et al., 1988). Thus, these diverticula might represent reservoirs of vesicle membrane that accumulate before endocytosis reaches its peak rate.

Volume of Rod Synaptic Cleft

The synaptic cleft can be defined as the extracellular space encountered by transmitter molecules before they are exposed to glial uptake. At conventional boutons housing single active zones, cleft volume is relatively small (~0.01 μm^3). The volume of the rod synaptic cleft is much greater because the invagination is deep (~1 μm) and also because surface areas of the invaginating processes are extensive. We calculated the cleft volume to be ~0.21 μm^3 (see Experimental Procedures). This is 20-fold greater than it is for the conventional bouton.

One consequence of the invagination is that all 4 postsynaptic processes are exposed to each quantum of transmitter before it reaches glia. A corollary is that the average glutamate concentration in the cleft due to one quantum would be 20-fold lower than at the standard bouton. However, the average concentration in the cleft does not reflect the peak concentration at the postsynaptic receptors (Clements et al., 1992), and that is the critical factor for binding. Thus, if glutamate receptors with different binding affinities were deployed judiciously within the cleft (see Discussion), one quantum might affect all 4 postsynaptic processes.

Discussion

Only the Rod Employs a Single Active Zone

The rod is the only known mammalian neuron whose total output of transmitter quanta occurs at a single active zone. Cone terminals employ ~20 active zones (e.g., Ahnelt et al., 1990), as do terminals of the large amphibian rods (e.g., Mariani, 1986). Comparable numbers are used by other ribbon terminals: 19 active zones at bullfrog hair cells (Roberts et al., 1990), 30 at the cat rod bipolar terminals (McGuire et al., 1984), 30–50 at monkey midget bipolar terminals (Calkins et al., 1994), and up to 105 at cat cone bipolar terminals (Cohen and Sterling, 1990). The number of active zones employed by motor axons and central axons is even greater—hundreds to thousands (e.g., Pumplin et al., 1981; Walrond and Reese, 1985; see Discussion of Gulyás et al., 1993). Thus, the rod's ability to manage with a single active zone is apparently unique in mammals and may reflect the irreducible simplicity of its message. Only the teleost rod—which like the mammal's is thin (Cajal, 1972) and thus may also transmit only a binary signal—has a single ribbon synapse (Stell, 1967; Saito et al., 1985; Hidaka et al., 1986).

The Mammalian Rod Synapse Is Large and Invariant

The rod active zone is the largest known in the central nervous system. Its 130 docking sites are more than twice that at the largest active zones of conventional synapses (Akert, 1973). The rod active zone in cat is also structurally invariant. It is always arched and of essentially fixed length (coefficient of variation = 0.13). Correspondingly, the ribbon is always crescent shaped and of fixed surface area (coefficient of variation = 0.19). Finally, the postsynaptic processes always constitute a tetrad. Even when the presynaptic structure appears "fractured" (Figure 3B), the total extents of active zone and ribbon along with the postsynaptic tetrad are preserved.

The rod synapse is also invariant across mammalian species. The overall size of the terminal is virtually the same from mouse to man. A single ribbon is present in rat, guinea pig, monkey, and rabbit; and it is crescent shaped in rat, guinea pig, and monkey (Ladman, 1958; Sjöstrand, 1958; McCartney and Dickson, 1985; Dacheux and Raviola, 1986; Townes-Anderson et al., 1988; our unpublished data). Some rods in monkey and human have been reported to have two or three ribbons (Missotten, 1965; Linberg and Fisher, 1988; Grünert and Martin, 1991). If (as in cat) these terminals resembled single-ribbon terminals in total depot and docking sites, they could be considered as single-ribbon terminals with fractured presynaptic apparatus.

The species invariance of rod presynaptic structure also seems to hold quantitatively. In guinea pig the active zone is 2.5 μm long, and the ribbon surface area is 0.5 μm^2 (Sjöstrand, 1958). In monkey the active zone is ~2.4 μm long, and the ribbon surface area is ~1.07 μm^2 ($n = 2$; unpublished data).

Such detailed conservation of form and size is certainly unusual and perhaps unique. For example, sympathetic ganglion neurons vary markedly across species in correlation with body size (Purves et al., 1985), and retinal ganglion cells vary markedly in size and branching pattern with eccentricity (Cajal, 1972). Even boutons from a single afferent fiber vary markedly in size, and in number and size of active zones (e.g., Yeow and Peterson, 1991; Pierce and Mendell, 1993). Thus, the strict conservation of rod synaptic structure may signify conservation of synaptic mechanism.

Hypothesis Relating Structure to Function at the Rod Synapse

We identify as a key design issue the fact that, while each rod carries the tiniest possible packet of information (a binary signal), the rod population is extremely dense (up to 500,000 per μm^2; Williams et al., 1993). Consequently, a rod's synaptic apparatus should be reliable but physically compact. The mammalian strategy has been to signify zero photoisomerizations with a high tonic rate of transmit-

ter release (calculated to be at least 40 vesicles per second; Rao et al., 1994) and one photoisomerization with a brief pause in release. This calculation assumes that every quantum evokes the standard all-or-none postsynaptic potential in all 4 postsynaptic processes. Thus, we hypothesize that the rod's presynaptic structure is specialized to maintain a high rate of tonic transmitter release, whereas the synaptic cleft and the arrangement of postsynaptic structures are specialized to maximize the effect of every released transmitter quantum. Our physical model of the rod synaptic terminal is summarized in Figure 5.

Presynaptic

Any faltering in the high quantal rate will tend to produce an extra-long interval between quanta indistinguishable from that caused by a photoisomerization (Rao et al., 1994). Such a spurious pause would evoke spikes from the ganglion cell, thus signaling a photon where there was none (false positive; Barlow et al., 1971; Mastronarde, 1983). Yet the combined evidence from physiology and circuitry (Baylor et al., 1984; Sterling et al., 1988) and from psychophysics (Sakitt, 1972) suggests that the rate of false positives is extremely low. If the high tonic rate is maintained by releasing vesicles from a pool of docking sites with equal and fixed release probability, each site must be reloaded promptly. Were vacant sites to accumulate, the mean rate would fall and the chances of an extra-long interval (i.e., a false positive) would rise.

The size of the rod active zone protects against extra-long intervals in two ways. First, the large number of docking sites would minimize the turnover rate at individual docking sites, and thus maximize the time available for each site to reload. Assuming 130 sites and a rate of 40 vesicles per second, mean turnover time would be 3.25 s. Second, if vacant sites did accumulate, each would constitute a small fraction of the total sites; thus, the large active zone would buffer fluctuations in tonic rate due to this source. However, since empty docking sites would be detrimental, maintaining the rod's high tonic release rate may depend critically on the mechanism for reloading.

An empty docking site on the presynaptic membrane presents a small target (~35 nm radius) for capture of a synaptic vesicle assumed to be diffusing in the cytoplasm. The ribbon presents a much broader target (equivalent radius ~500 nm) for vesicle capture. Since the capture rate by a "disk-like adsorber" is proportional to the radius (Berg, 1983), the ribbon (a two-sided disk) will be 30-fold more efficient than a docking site. Because the basal edge of the two-dimensional ribbon conforms to the one-dimensional active zone (Figure 5), any vacant docking site can be reloaded simply by translocation of a vesicle 48 nm along the ribbon. Over this short distance, diffusion is rapid. Such tricks of facilitating capture of particles in random motion are well known in bacteria (Berg, 1983). However, this is the first instance (to our knowledge) in which the principles appear to operate at the level of an intracellular organelle.

Postsynaptic

In contrast to the conventional bouton where the synaptic cleft is two-dimensional, the cleft at the rod synapse is large and three-dimensional (Figure 1A versus Figure 5). This design seems necessary to accommodate 4 postsynaptic processes. However, not all processes can be equally close to the sites of transmitter release. This problem seems to be addressed by two different adaptations.

First, the horizontal cells located near the docking sites bear low affinity AMPA/kainate receptors (EC_{50} = 1 mM; Hestrin, 1992), whereas the bipolar cell dendrites located much farther away bear high affinity APB receptors (EC_{50} = 10 μM; de la Villa et al., 1995). Second, distance from the docking sites to the low affinity receptors is held constant by the fit of horizontal cell processes to the curve of the active zone (Figures 4A and 4B; Figure 5). Distance to the high affinity receptors is not so rigidly regulated, possibly because at long distances the peak glutamate concentration varies little (unpublished data). However, the arch of the active zone creates a radius roughly centered on the bipolar cell dendrites (Figure 5). This tends to minimize differences in the distance to target for all docking sites, minimizing differences in effectiveness. This would be especially true if the postsynaptic receptors were not concentrated focally at the dendritic tip but distributed evenly along the whole invaginating segment.

In short, the presynaptic architecture seems designed to sustain a high tonic rate of release; the postsynaptic architecture seems designed to allow every vesicle to affect all 4 processes. This saves the extra volume that would be needed for four separate active zones if standard boutons were employed. These hypotheses regarding the functional architecture now require quantitative evaluation.

Experimental Procedures

An adult cat was deeply anesthetized with pentobarbital (45 mg/kg). One eye was dilated with atropine and exposed to moderately bright light (ambient illumination > 50 cd/m^2), while the other eye was fitted with a black plastic contact lens and the lid sutured so that no light could enter this eye directly. For light to leak into the occluded eye via the open one, it would have to penetrate the sclera and pigmented choroid of both eyes, plus the bony orbit covered on both sides by connective tissue. Thus, light attenuation, if not complete, was probably at least 4 log units, well into the scotopic range. At about 3 p.m., after 2 hr of adaptation to these conditions, the animal was perfused with a phosphate-buffered mixture of 1% glutaraldehyde/1% paraformaldehyde followed by 2% glutaraldehyde/2% paraformaldehyde. The retina was postfixed in osmium tetroxide, stained with uranyl acetate, dehydrated, and embedded in Epon. Tissue from the area centralis of the retina was cut into a series of ultrathin sections (0.09 μm). The dark-adapted tissue was cut radially into a series of 59 sections, and the light-adapted tissue was cut tangentially into a series of 85 sections. Sections were poststained with uranyl acetate and lead citrate and photographed at 5000× in an electron microscope.

Ribbon synapses were counted in 75 dark-adapted and 260 light-adapted rod terminals from this cat and in 50 terminals from two other cats. Further detailed measurements were taken from the rods subjected to light and dark adaptation. The presynaptic ribbon was reconstructed in 13 dark-adapted and 13 light-adapted terminals. For 16 of these terminals (8 dark- and 8 light-adapted), all presynaptic and postsynaptic structures were reconstructed and the cleft features were measured wherever possible. Table 1 shows the measurements only for the rod terminals that housed single presynaptic ribbons.

Rod terminals were reconstructed by tracing their profiles in successive sections onto acetate sheets aligned on a cartoonist's jig. These tracings were then digitized and "stacked" by a personal computer. Active zone length and distance between active zone and bipolar cell dendrite were measured from views of the three-dimensional images taken parallel and perpendicular to the plane of the synaptic ribbon.

Surface areas of the ribbon, the rod processes, and the postsynaptic processes were computed by multiplying the perimeter of profiles in a section by the section thickness and summing this value across sections. The volumes of the rod and postsynaptic processes were computed by multiplying the surface area of profiles in a section by the section thickness and summing this across sections. The cleft volume in the invagination was calculated by summing the surface areas of the 4 postsynaptic processes and subtracting out the surface areas that had been counted twice (i.e., the surface areas where the processes apposed each other), and then multiplying this area by the cleft width (16 nm). The physical model of a typical rod terminal was constructed from thin slabs of modeling clay shaped to represent profiles in successive sections.

Acknowledgments

All correspondence should be addressed to P. S. We are grateful for many helpful comments on an early draft of this paper by Drs. A. J. Hudspeth, Fred Rieke, and Brian Boycott. This work was supported by National Eye Institute grants EY00828 and EY08124.

The costs of publication of this article were defrayed in part by the payment of page charges. This article must therefore be hereby marked *"advertisement"* in accordance with 18 USC Section 1734 solely to indicate this fact.

Received November 10, 1994; revised January 19, 1995.

References

Abe, H., and Yamamoto, T. Y. (1988). Modification of diurnal changes in the ultrastructure of synaptic ribbons of the turtle. Tohoku J. Exp. Med. *156*, 381–393.

Ahnelt, P., Keri, C., and Kolb, H. (1990). Identification of pedicles of putative blue-sensitive cones in the human retina. J. Comp. Neurol. *293*, 39–53.

Akert, K. (1973). Dynamic aspects of synaptic ultrastructure. Brain Res. *49*, 511–518.

Attwell, D. (1986). Ion channels and signal processing in the outer retina. Quart. J. Exp. Physiol. *71*, 497–536.

Barlow, H. B., Levick, W. R., and Yoon, M. (1971). Responses to single quanta of light in retinal ganglion cells of the cat. Vision Res. *S3*, 87–101.

Baylor, D. A., Nunn, B. J., and Schnapf, J. L. (1984). The photocurrent, noise and spectral sensitivity of rods of the monkey *Macaca fascicularis*. J. Physiol. *357*, 575–607.

Berg, H. C. (1983). Random Walks in Biology (Princeton: Princeton University Press).

Boycott, B. B., and Kolb, H. (1973). The connections between bipolar cells and photoreceptors in the retina of the domestic cat. J. Comp. Neurol. *148*, 91–114.

Brandon, C., and Lam, D. M. K. (1983). The ultrastructure of rat rod synaptic terminals: effects of dark-adaptation. J. Comp. Neurol. *217*, 167–175.

Cajal, S. R. (1972). The Structure of the Retina (Springfield, Illinois: Charles C. Thomas).

Calkins, D. J., Schein, S. J., Tsukamoto, Y., and Sterling, P. (1994). M and L cones in macaque fovea connect to midget ganglion cells by different numbers of excitatory synapses. Nature *371*, 70–72.

Ceccarelli, B., Hurlbut, W. P., and Iezzi, N. (1988). Effect of α-latrotoxin on the frog neuromuscular junction at low temperature. J. Physiol. *402*, 195–217.

Clements, J. D., Lester, R. A. J., Tong, G., Jahr, C. E., and Westbrook, G. L. (1992). The time course of glutamate in the synaptic cleft. Science *258*, 1498–1501.

Cohen, A. I. (1964). Some observations on the fine structure of the retinal receptors of the American gray squirrel. Invest. Ophthalmol. *3*, 198–216.

Cohen, E., and Sterling, P. (1990). Demonstration of cell types among cone bipolar neurons of cat retina. Philos. Trans. Roy. Soc. Lond. (B) *330*, 305–321.

Dacheux, R. F., and Raviola, E. (1986). The rod pathway in the rabbit retina: a depolarizing bipolar and amacrine cell. J. Neurosci. *6*, 331–345.

de la Villa, P., Kurahashi, T., and Kaneko, A. (1995). L-glutamate-induced responses and cGMP-activated channels in retinal bipolar cells dissociated from the cat. J. Neurosci., in press.

Dowling, J. E. (1991). The retina. In Encyclopedia of Human Biology (New York: Academic Press), pp. 615–631.

Evans, E. M. (1966). On the ultrastructure of the synaptic region of visual receptors in certain vertebrates. Zeitschrift für Zellforschung *71*, 499–516.

Gray, E. G., and Pease, H. L. (1971). On understanding the organisation of the retinal receptor synapses. Brain Res. *35*, 1–15.

Grünert, U., and Martin, P. R. (1991). Rod bipolar cells in the macaque monkey retina: immunoreactivity and connectivity. J. Neurosci. *11*, 2742–2758.

Gulyás, A. I., Miles, R., Sík, A., Tóth, K., Tamamaki, N., and Freund, T. F. (1993). Hippocampal pyramidal cells excite inhibitory neurons through a single release site. Nature *366*, 683–687.

Hestrin, S. (1992). Activation and desensitization of glutamate-activated channels mediating fast excitatory synaptic currents in the visual cortex. Neuron *9*, 991–999.

Hidaka, S., Christensen, B. N., and Naka, K.-I. (1986). The synaptic ultrastructure in the outer plexiform layer of the catfish retina: a three-dimensional study with HVEM and conventional EM of Golgi-impregnated bipolar and horizontal cells. J. Comp. Neurol. *247*, 181–199.

Kolb, H. (1977). The organization of the outer plexiform layer in the retina of the cat: electron microscopic observations. J. Neurocytol. *6*, 131–153.

Ladman, A. J. (1958). The fine structure of the rod-bipolar cell synapse in the retina of the albino rat. J. Biophys. Biochem. Cytol. *4*, 459–465.

Linberg, K. A., and Fisher, S. K. (1988). Ultrastructural evidence that horizontal cell axon terminals are presynaptic in the human retina. J. Comp. Neurol. *268*, 281–297.

Mariani, A. P. (1986). Photoreceptors of the larval tiger salamander retina. Proc. Roy. Soc. Lond. (B) *227*, 483–492.

Massey, S. C. (1990). Cell types using glutamate as a neurotransmitter in the vertebrate retina. In Progress in Retinal Research, Vol. 9, N. N. Osborne and G. Chader, eds. (London: Pergamon Press), pp. 399–425.

Mastronarde, D. N. (1983). Correlated firing of cat retinal ganglion cells. II. Responses of X- and Y-cells to single quantal events. J. Neurophysiol. *49*, 325–349.

McCartney, M. D., and Dickson, D. H. (1985). Photoreceptor synaptic ribbons: three-dimensional shape, orientation and diurnal (non) variation. Exp. Eye Res. *41*, 313–321.

McGuire, B. A., Stevens, J. K., and Sterling, P. (1984). Microcircuitry of bipolar cells in cat retina. J. Neurosci. *4*, 2920–2938.

Missotten, L. (1965). The Ultrastructure of the Human Retina (Brussels: Editions Arscia S. A.).

Nomura, A., Shigemoto, R., Nakamura, Y., Okamoto, N., Mizuno, N., and Nakanishi, S. (1994). Developmentally regulated postsynaptic localization of a metabotropic glutamate-receptor in rat rod bipolar cells. Cell *77*, 361–369.

Pierce, J. P., and Mendell, L. M. (1993). Quantitative ultrastructure of Ia boutons in the ventral horn: scaling and positional relationships. J. Neurosci. *13*, 4748–4763.

Pumplin, D. W., and Reese, T. S. (1978). Membrane ultrastructure of the giant synapse of the squid Loligo pealei. Neuroscience *3*, 685–696.

Pumplin, D. W., Reese, T. S., and Llinàs, R. (1981). Are the presynaptic membrane particles the calcium channels? Proc. Natl. Acad. Sci. USA *78*, 7210–7213.

Purves, D., Rubin, E., Snider, W. D., and Lichtman, J. (1985). Relation of animal size to convergence, divergence, and neuronal number in peripheral sympathetic pathways. J. Neurosci. *6*, 1–5.

Rao, R., Buchsbaum, G., and Sterling, P. (1994). Rate of quantal transmitter release at the mammalian rod synapse. Biophys. J. *67*, 57–63.

Raviola, E. (1976). Intercellular junctions in the outer plexiform layer of the retina. Invest. Ophthalmol. *15*, 881–895.

Raviola, E., and Gilula, N. B. (1975). Intramembrane organization of specialized contacts in the outer plexiform layer of the retina. J. Cell Biol. *65*, 192–222.

Ripps, H., and Chappell, R. L. (1991). Ultrastructural and electrophysiological changes associated with K^+-evoked release of neurotransmitter at the synaptic terminals of skate photoreceptors. Vis. Neurosci. *7*, 597–609.

Roberts, W. M., Jacobs, R. A., and Hudspeth, A. J. (1990). Colocalization of ion channels involved in frequency selectivity and synaptic transmission at presynaptic active zones of hair cells. J. Neurosci. *10*, 3664–3684.

Saito, T., Kujiraoka, T., Yonaha, T., and Chino, Y. (1985). Reexamination of photoreceptor-bipolar connectivity patterns in carp retina: HRP-EM and Golgi-EM studies. J. Comp. Neurol. *236*, 141–160.

Sakitt, B. (1972). Counting every quantum. J. Physiol. *223*, 131–150.

Schaeffer, S. F., and Raviola, E. (1978). Membrane recycling in the cone cell endings of the turtle retina. J. Cell Biol. *79*, 802–825.

Sjöstrand, F. S. (1958). Ultrastructure of retinal rod synapses of the guinea pig eye as revealed by three-dimensional reconstructions from serial sections. J. Ultrastruct. Res. *2*, 122–170.

Smith, R. G., Freed, M. A., and Sterling, P. (1986). Microcircuitry of the dark-adapted cat retina: functional architecture of the rod-cone network. J. Neurosci. *6*, 3505–3517.

Spadaro, A., de Simone, I., and Puzzolo, D. (1978). Ultrastructural data and chronobiological patterns of the synaptic ribbons in the outer plexiform layer in the retina of albino rats. Acta Anat. *102*, 365–373.

Stell, W. K. (1967). The structure and relationships of horizontal cells and photoreceptor-bipolar synaptic complexes in goldfish retina. Am. J. Anat. *121*, 401–424.

Sterling, P. (1990). Retina. In The Synaptic Organization of the Brain, G. M. Shepherd, ed. (New York: Oxford University Press), pp. 170–213.

Sterling, P., Cohen, E., Freed, M. A., and Smith, R. G. (1987). Microcircuitry of the On-beta ganglion cell in daylight, twilight, and starlight. Neurosci. Res. *S6*, 269–285.

Sterling, P., Freed, M. A., and Smith, R. G. (1988). Architecture of the rod and cone circuits to the *On*-beta ganglion cell. J. Neurosci. *8*, 623–642.

Townes-Anderson, E., Dacheux, R. F., and Raviola, E. (1988). Rod photoreceptors dissociated from the adult rabbit retina. J. Neurosci. *8*, 320–331.

Vollrath, L., Meyer, A., and Buschmann, F. (1989). Ribbon synapses of the mammalian retina contain two types of synaptic bodies—ribbons and spheres. J. Neurocytol. *18*, 115–120.

Wagner, H.-J., and Djamgoz, M. B. A. (1993). Spinules: a case for retinal synaptic plasticity. Trends Neurosci. *16*, 201–206.

Walrond, J. P., and Reese, T. S. (1985). Structure of axon terminals and active zones at synapses on lizard twitch and tonic muscle fibers. J. Neurosci. *5*, 1118–1131.

Williams, R. W., Cavada, C., and Reinoso-Suárez, F. (1993). Rapid evolution of the visual system: a cellular assay of the retina and dorsal lateral geniculate nucleus of the Spanish wildcat and the domestic cat. J. Neurosci. *13*, 208–228.

Yamashita, M., and Wässle, H. (1991). Responses of rod bipolar cells isolated from the rat retina to the glutamate agonist 2-amino-4-phosphonobutyric acid (APB). J. Neurosci. *11*, 2372–2382.

Yeow, M. B. L., and Peterson, E. H. (1991). Active zone organization and vesicle content scale with bouton size at a vertebrate central synapse. J. Comp. Neurol. *307*, 475–486.